AIAA SciTech Forum
7-11 January 2019, San Diego, California
AIAA Scitech 2019 Forum

10.2514/6.2019-1137

An Experimental Investigation of the Effect of Surface Perforation on Unsteady Aerodynamic Force Reduction for a Hollow Cylinder

Vignesh kumar Sudalaimuthu[1]
San Diego State University, San Diego, CA, 92182-1308

and

Xiaofeng Liu[2]
San Diego State University, San Diego, California, 92182-1308

The effect of uniformly-distributed perforated holes on the surface of a hollow circular cylinder in reducing unsteady aerodynamic force has been investigated experimentally in a subsonic wind tunnel at four different Reynolds numbers from 0.5×10^5 to 2.0×10^5 based on a freestream velocity from 5m/s to 20m/s (at an increment of 5m/s) and circular cylinder diameter of 0.152m. The aerodynamic force was measured at a sample rate of 10,000 samples per second with a duration of 60 seconds using a 6-component load cell. The power spectrum, the mean and the r.m.s values of the drag, lift, and cylindrical axial force coefficients based on 6,000,000 measurement samples were acquired by repeating test 10 times for each Reynolds number. Comparisons indicate that the perforated cylinder with an 8% porosity and a hole diameter of about 2% of that of the cylinder gives both substantially less unsteady drag and lift than those of the smooth cylinder for the entire Reynolds number range tested, with the r.m.s. force reduction from 8% to 82% for the drag and 64% to 85% for the lift. Consistent with the above results, power spectral analysis of the force measurement signals indicates that there is an overall reduction in fluctuation amplitude across the spectrum for the perforated cylinder when compared with the smooth cylinder. The uncertainty analysis results confirm that the amount of reduction in force coefficients are beyond the error range, hence proving the effectiveness of perforated holes in unsteady force reduction. To further confirm the load cell measurement results, a hot-wire wake survey has been conducted at 5 different measurement stations downstream of the cylinder model. The results show that, significant reductions for velocity r.m.s. fluctuations were achieved for the perforated cylinder in comparison with the smooth one, with 9% reduction at the edge of the wake and 32% reduction at the center of the wake. Also, comparison of the hot-wire velocity spectrum results at different lateral locations at a near wake measurement station indicates a 12% to 76% reduction in the u-component normal stress, consistent with the force measurement results. Further investigations will be conducted by detailed flow field survey on the same models using stereo PIV (particle image velocimetry) measurement.

Nomenclature

C_p	=	pressure coefficient
Cx	=	force coefficient in the x direction
C_D	=	coefficient of drag
C_L	=	coefficient of lift
C_S	=	coefficient of cylindrical axial direction force

[1]Graduate Student, Department of Aerospace Engineering, SDSU. AIAA Student Member.
[2]Assistant Professor, Department of Aerospace Engineering, SDSU. AIAA Associate Fellow. Email: Xiaofeng.Liu@sdsu.edu

d	=	diameter of the cylinder
b	=	length of the cylinder
Fx	=	x component of force acting on the load cell
Fy	=	y component of force acting on the load cell
Fz	=	z component of force acting on the load cell
P	=	power spectral density
f	=	frequency
f_{max}	=	maximum frequency on the spectrum
Re	=	Reynolds number based on cylinder diameter and free stream velocity
ρ	=	density of the air in kg/m^3
U_∞	=	free stream velocity
U_{RMS}	=	root mean square of the velocity at particular location

I. Introduction

CIRCULAR cylinder type of structures can be found in a variety of applications such as smoke chimney, cable-stayed bridges and support structures in ocean engineering, etc. Dangerously large vibration caused by asymmetric vortex shedding is a major problem in using smooth circular cylinder in these fields (Price[1], 1956). There are nearly ten decades of research work that have been conducted by various researchers to reduce the unsteady aerodynamic force acting on circular cylinders (e.g., Pinar *et al.*[2], 2015). The unsteadiness of aerodynamic force acting on a circular cylinder is primarily due to asymmetric vortex shedding that further forms well-known Karman Vortex street[3] (Homann, 1936). Unsteady aerodynamic force behind the smooth cylinder causes flow induced vibration. This phenomenon can be visualized in the hoisted flag, as the flag keeps on waving in simultaneous motion (Price[1], 1956). Copious amount of research have been conducted in this area to reduce the vibration acting on the cylinder at broad spectrum of Reynolds number. The exposure of vibration acting on the model over a long period can cause severe damage and may even cause structural failure. Transition Reynolds number of 1.0×10^5 to 3.0×10^5 is the range in which there is a sudden drop in force coefficient (Zdravkovich[4], 1990). This range of Reynolds number gives higher unsteadiness in the flow. Thus, the current research work focuses on this Reynolds number range, aiming to verify the effectiveness of the surface perforation method in reducing the unsteady, flow-induced vibrations acting on bluff bodies in that Reynolds number range.

Flow around the cylinder acts differently as the Reynolds number changes. Conventionally, the flow patterns were divided into three Reynolds number regions, namely sub-critical, critical, and super-critical regions. Also, there are three types of transitions: in-the-near-wake, along the free shear layer and along the boundary layer. Zdravkovich[4] (1990) further argured based on observation that flows past a circular cylinder can be characterized by 15 flow regimes, spanning the Reynolds number range from 10^0 to 10^8 with disturbance free flow. Lin *et. al*.[5] (1995) conducted near-wake survey at $Re = 5.0\times10^3$ to 1.0×10^4 and, with an emphasis on the relationship between the structures of shear layer separation from cylinder to large-scale vortex formation, found that the small-scale Kelvin-Helmholtz vortices are embedded within large-scale Karman vortices. Norberg[6] (1998) shows that there is a fundamental transition occurring in the near wake region between Re 5×10^3 to 1×10^4, where mean wave closure point moves upstream by 0.8 diameters. In the same Reynolds number range Rajagopalan and Antonio[7] (2005), measured the occurrence of Kelvin-Helmholtz vortex. They also found less organized vortex shedding at Re > 5000 and well-organized vortex shedding at Re < 5000. Dong *et al.*[8] (2006) proves that with change in Reynolds number, the shear layer instability changes. At Re = 3900, shear layer velocity spectra shows a sharp broadband peak, whereas at Re =10,000, shear layer velocity spectra give 'Plateau' type peak, also this follows the power law $Re^{0.67}$ as suggested by Prasad and Williamson[9] (1997). The peak Turbulence Kinetic Energy (T.K.E.) occurs at the saddle point of the flow patterns for cylinder whereas, 2 peak T.K.E occurs for sphere due to the 3D flow behavior (Ozkan *et. al.*[10], 2011).

As summarized by Price[1] (1956), among various types of geometries, the perforated shroud configuration seems to be more effective in reducing the vibration of the circular cylinder. Vibration amplitude of the shrouded circular cylinder is small compared to the plain circular cylinder, in the same time the large amplitudes were inhibited. The drag of the shroud cylinder doesn't seem to be affected by the Reynolds number effect in the transitional and super-critical range ($1.3\times 10^5 < Re < 4.3\times 10^5$), but the increment of the gap between the circular cylinder and the shroud increases the drag value. Basir Sahin and his group (Ozkan *et.al.*[11], 2017; Ozkan *et.al.*[12], 2012; Gozman *et.al.*[13], 2013; Pinar *et.al.*[14], 2017; Durhasan *et.al.*[15], 2016) have conducted several experiments on circular cylinder with perforated shrouds at Reynolds number range of 3.0×10^3 to 1.0×10^4. One of which is a water tunnel experiment on circular cylinder with perforated shroud at different shroud porosity and reported the reduction in turbulence kinetic energy (T.K.E.) and Reynolds stress (Ozkan *et al.*[12], (2012)). PIV flow measurement shows that the interaction of shear layer of the inner cylinder has been prevented by the outer cylinder, which in-turn significantly reduces the vibration of the inner cylinder. Also, the optimal gap between inner and outer cylinder has been identified. The vortex shedding has been reduced by perforated shroud for circular cylinders, but at the price of increased weight and drag value. Chen[16] (2013) performed wind tunnel experiment on circular cylinder with rectangular slots distributed evenly at Reynolds number of 4.16×10^4. For different porosity (passive-suction ports) the optimum porosity of has been achieved for passive suction rate of 0.1524 configuration. The fluctuating amplitude reduction for lift coefficient and mean drag coefficient reduction was observed in that experiment. Also, the T.K.E. is smaller for this case and a decrement in vortex shedding frequency was observed. Pinar *et. al.*[2] (2015) studied the effect of porosity on a hollow circular cylinder at Reynolds number of 10,000. The PIV measurement results show that an elongation in shear layer, fluctuation attenuation and prevention of Karman vortex street formation occurring in that flow. As porosity increases from 0.1 to 0.8, the reduction in vorticity increases from 17% to 42%.

It is conceived that perforation holes evenly allocated throughout the circular cylinder surface would improve the effectiveness in unsteady aerodynamic force reduction. Most research work on perforated circular cylinder has been conducted at very low Reynolds numbers (Re ~ 10^3 – 10^4). At critical Reynolds number range the flow properties around the cylinder is very sensitive to variation in Reynolds number. Thus the current research work has been conducted in the critical Reynolds number range to elucidate the effect of surface perforation on unsteady force reduction on circular cylinder at that Reynolds number range.

The scope of this paper is as follows. The chapter II covers the experimental setup of the circular cylinder in the wind tunnel and its configurations. Comparison of the results from force measurements, hot-wire wake survey and uncertianty analysis between smooth and perforated cylinders are discussed in detailed manner in chapter III. The chapter IV summarizes the research work and presents the conclusion.

II. Experimental Procedure

The experiment is conducted in a closed-loop subsonic wind tunnel at San Diego State University. The tunnel has a test-section size of 1.14 m (W) $\times$ 0.81 m (H) $\times$ 1.70 m (L). Airflow in the wind tunnel is generated by means of a 150 HP constant speed electric motor driving a variable-pitch, 4-bladed propeller. This system provides for a continuously variable speed range in the test section from 0 to 180 mph (i.e., 0 – 80 m/s). The length of the test section is kept transparent using plexi-glasses on both sides. The cylinder models are mounted vertically at the center of the test-section floor with 4 inches clearance from the top and bottom tunnel walls. The testing is conducted on smooth and perforated cylinders at 5, 10, 15 and 20 m/s tunnel speed, with corresponding Reynolds numbers ranging from 0.5×10^5 to 2.0×10^5. The turbulence factor in the test section is 1.27 (i.e., turbulence intensity about 0.3%).

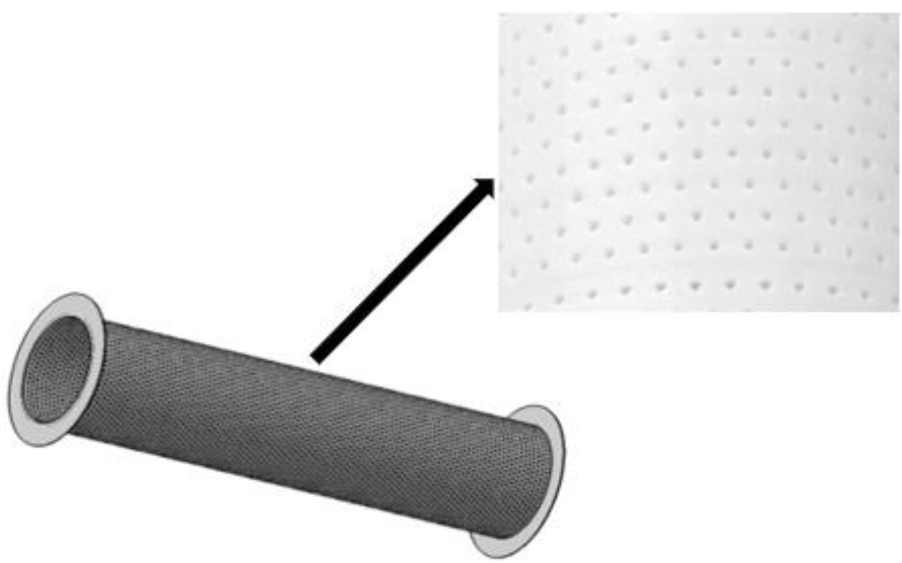

Figure 1 Perforated cylinder designed using SolidWorks.

A hollow smooth cylinder with 6-inch diameter, 24-inch length and 0.1875-inch thickness is designed using SolidWorks. This design is then printed with plastic material at the SDSU 3D printing facility. End plates are attached to both ends of the circular cylinder model to ensure the flow past the cylinder is two dimensional in the mean. The blockage ratio of the cylinder model is 10% with respect to the frontal area of the test section. Uniformly distributed circular holes with 2 mm diameter (~1.3% of cylinder diameter) are perforated on the surface of the circular cylinder with holes spacing at an azimuthal angel of 5 degrees apart circumferentially as shown in Figure 1. The porosity of the cylinder is 8.25%.

Two types of measurement techniques are involved in the investigation. Firstly, an ATI MINI-45, 6-component load cell is used to measure the forces acting on the model. The load cell is mounted under the floor of the wind tunnel test section, which is connected through 2 support rods to the cylinder model as shown in Figure 2. The Maximum capacity of the load cell is $F_x = F_y =$ 580N and F_z=1160N for forces, and T_x=T_y=T_z=20Nm for torques,. For each velocity, the test has been repeated for 10 runs. Each run consists of 600,000 samples acquired at a sampling rate of 10kHz for 60 seconds. Thus, at each tunnel speed, a total of 6,000,000 samples have been acquired. For each set of data acquired, drag, lift and axial force are measured. Finally, power spectral density is calculated and compared for both configurations. Secondly, a TSI 300 Constant Temperature Anemometer is used to measure the downstream wake velocity profile

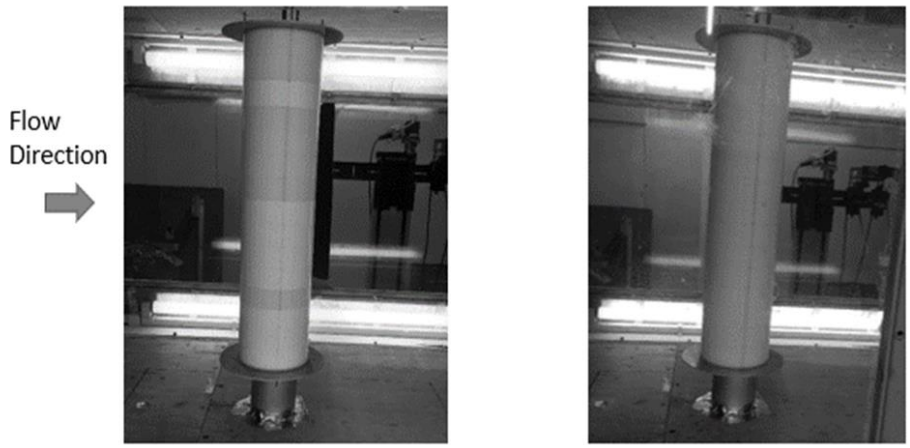

(a) **(b)**

Figure 2 Experimental setup of (a) smooth cylinder and (b) perforated cylinder.

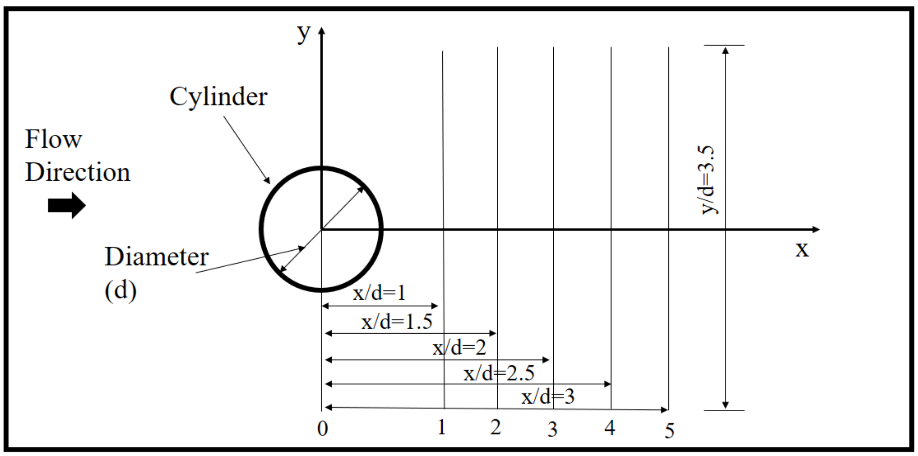

Figure 3 Location of the measurement stations in the hot-wire flow survey.

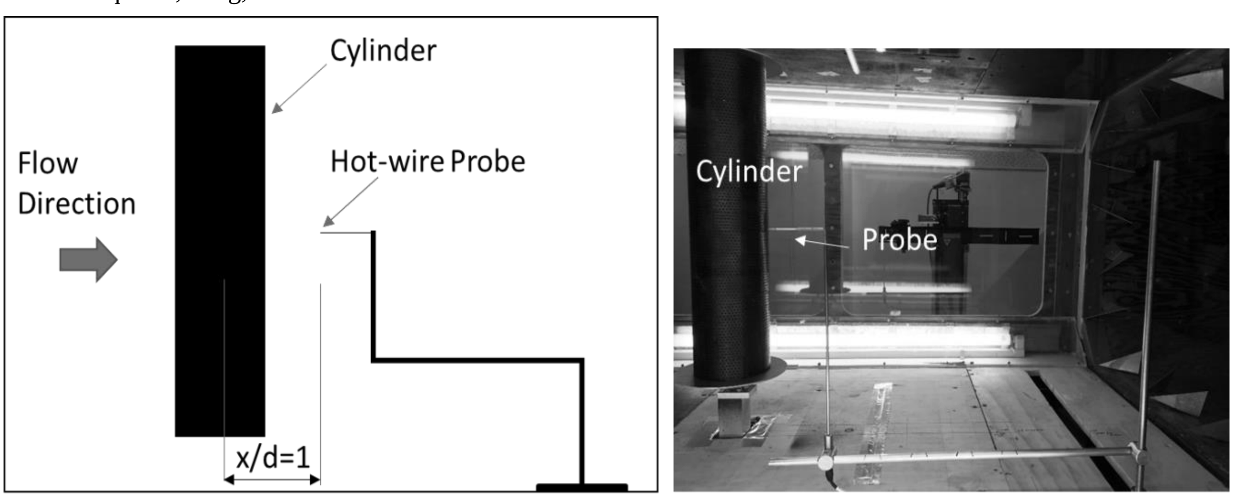

Figure 4 Wind tunnel hot-wire survey probe set-up

behind each cylinder model as shown in Figure 3 and Figure 4. The sampling rate is 15,000 Hz and total number of samples at each measurement point is 900,000. A National Instruments USB-6003 analog to digital converter is used to convert the hot wire voltage signals through which the wake-velocity is calculated at five downstream locations. The measuremn stations are located at x/d = 1.0, 1.5, 2.0, 2.5 and 3.0, respectively. At each downstream location, velocity profiles are measured starting from y/d = -3.0 to 3.0.

III. Results and Discussion

A. Load cell force measurement results

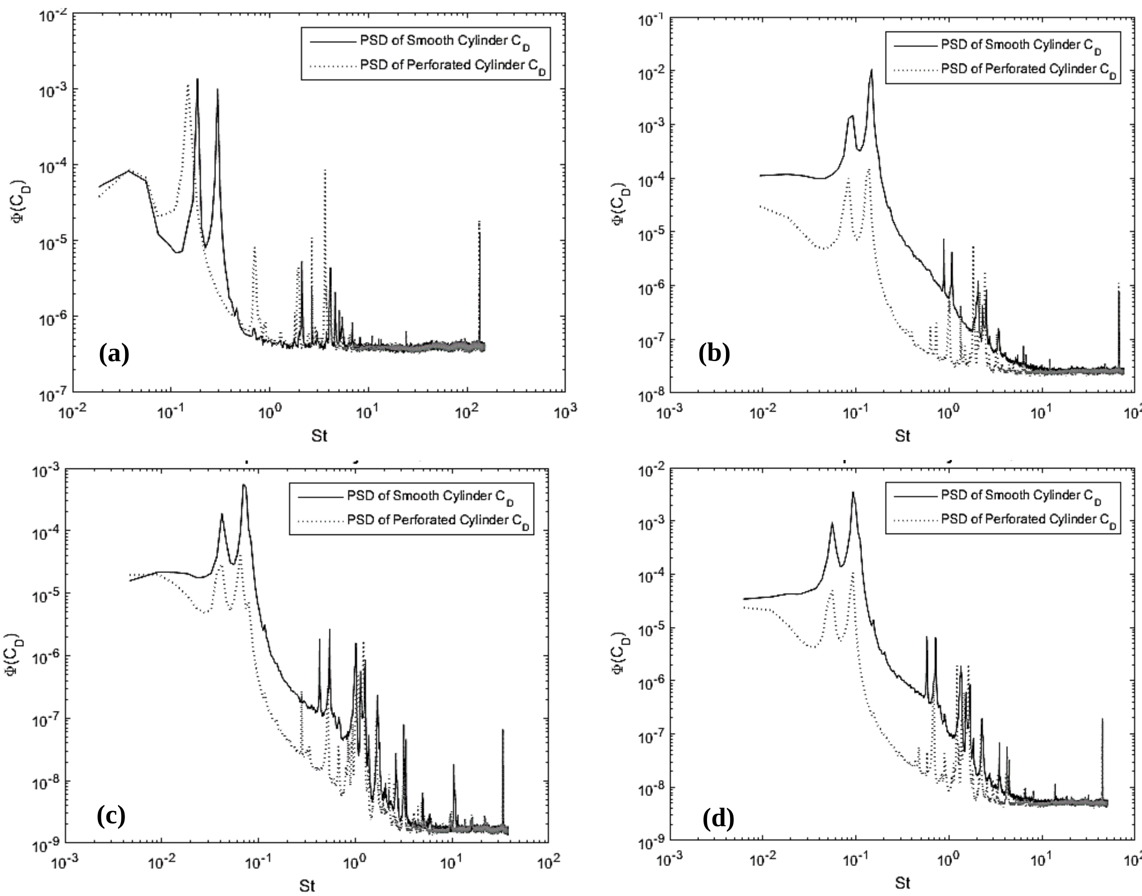

Figure 5 Comparisons of the Power Spectral Density of Drag Coefficient vs. Strouhal number for the smooth and perforated cylinders acquired at free stream velocities of (a) 5m/s, (b) 10m/s, (c) 15m/s and (d), 20m/s, respectively.

Figure 5 shows the comparison of the Power Spectral Density (PSD) of the drag coefficient C_D vs. Strouhal number ($St=fL/U_\infty$) of the smooth cylinder with that of the perforated cylinder. The PSD distributions over a period of 10 minutes has been averaged. As expected, the smooth cylinder case shows higher peak PSD values in comparison with the perforated one. When the r.m.s. values are compared, there is an 8.72%, 81.82%, 78.96% and 61.48% reduction at Reynolds numbers of 0.5×10^5, 1.0×10^5, 1.5×10^5, and 2.0×10^5, respectively. This implies that, a perforated cylinder with only 8% porousity will have a substantial reduction in flow induced vibration. The PSD plots show that there is a high peak occurring at St = 0.2, which corresponds to the shedding frequency of the cylinder at this Reynolds number range as given in White[17] (2011). The reduction in PSD amplitude at the shedding frequency for the perforated cylinder suggests a reduction in the Karman Vortex intensity and hence the vibration. Similarly, in Figure 6, the PSD plots of the lift coefficient C_L for all 4 Reynolds number show a significant reduction of 63.76%, 84.55%, 82.84% and 67.48% in r.m.s. values of C_L at 5, 10, 15 and 20m/s free stream velocities, respectively. Reduction in vibration can also be visually seen when the test is being conducted. The smooth cylinder vibrates significantly at free stream velocities of 10 to 20m/s while the perforated cylinder has almost unnoticeable vibration.

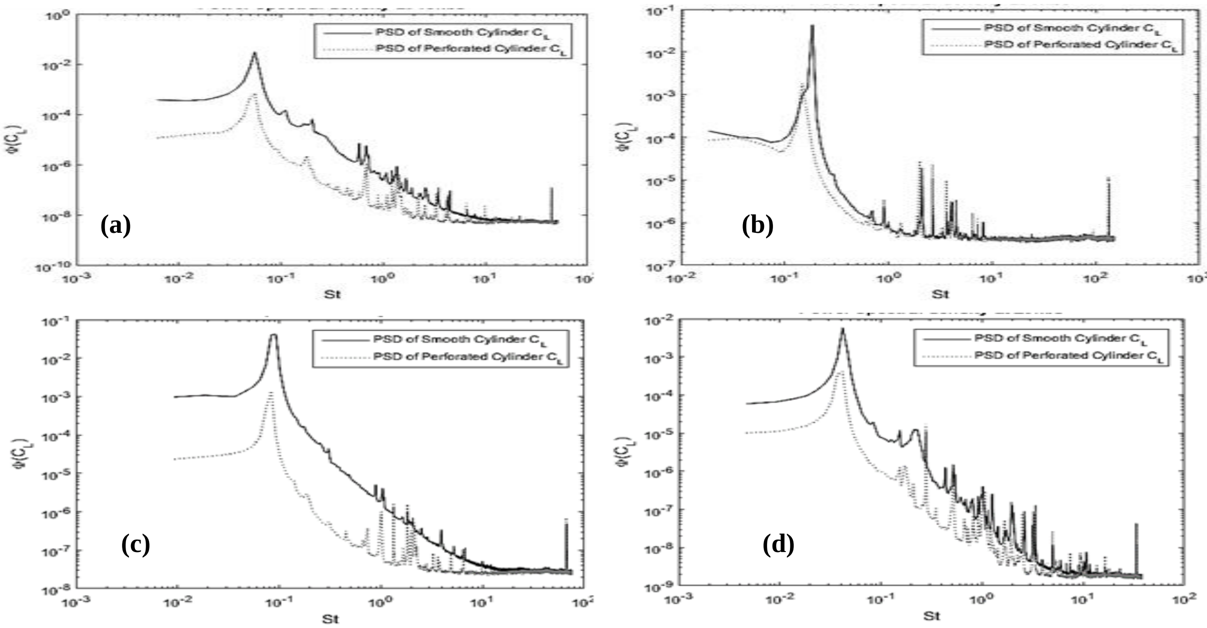

Figure 6 Power Spectral Density of Lift Coefficient vs. Strouhal number of the smooth and perforated cylinders for 5, 10, 15, 20m/s velocities as given in figures (a), (b), (c) and (d) respectively.

Figure 7 shows the comparison of the mean drag coefficients of the smooth and perforated cylinders with Wieselsberger[18] (1922) classic drag coefficient data for Reynolds number range of 10^4 to 10^5. Overall reduction in mean drag can be seen in the Figure 12 This implies that the smooth cylinder is not as smooth as the cylinder used in reference; because it has more roughness (k/d=0.001) which causes the reduction in drag coefficient for the smooth cylinder. Also, this roughness effect is confirmed with the classic drag coefficient data for roughness of k/d=0.001, as shown in Figure 7. The error bar indicates that the uncertainty level is in good range where the perforated cylinder results don't interact with the smooth cylinder results. Thus, the results are not influenced by uncertainty in the flow measurements.

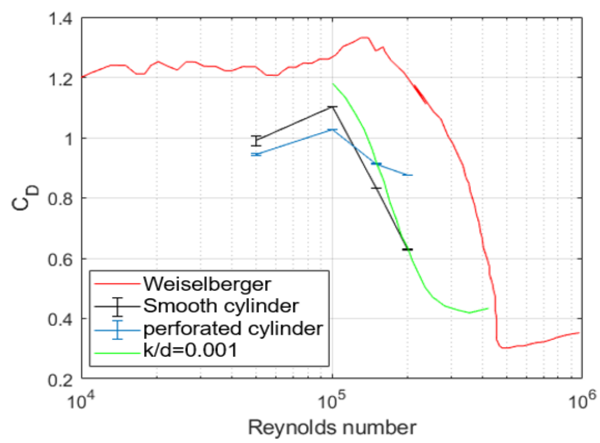

Figure 7 Comparison of Weiselberger [35] classical drag coefficient curve with the mean drag coefficient of the current experiment.

From the PSD plots of C_D, and C_L, (Figures 5 and 6) it can be seen that there are many low amplitude peaks occurring in the high frequency range of 0.2 <*St* <20. Hence impact test is conducted for both cylinder models without turning the velocity on. At 0m/s wind speed, the cylinder has been damped using a rod (cylinder mounted inside the tunnel). Then the load variation was measured using load cell, just like the wind tunnel testing. This procedure was repeated 10 times and ensemble average has been taken to calculate the Power spectral density. In this way, the natural vibration of the structures of the smooth and the perforated cylinder can be identified.

Figure 8 shows the PSD plot for drag coefficient acquired at 10m/s in comparison with the impact test with 0m/s velocity on the right. The peak values are noted on both plots. It can be seen that other than the shedding frequency, all other peaks occurring at the PSD plot of the 10m/s test result coincide with the natural vibrating frequency of the cylinder structure. Figure 9 compares the PDF of the lift coefficients with the corresponding impact test result. In this case also there is an agreement in the relevant peak values between the wind-on and wind-off tests. The matched peaks represents the natural structural vibrating frequencies. Similarly, the Side force coefficient was compared in figure 10, and the matched frequencies corresponds to the natural frequency of the cylinder model structure.

As shown in Figures 8(a), 9(a) and 10(a), most of the unsteady force reduction occurs at the low frequency range. For force signals low pass filtered at 100 Hz, the magnitudes of the fluctuation energy for the drag, lift and the side force on the perforated cylinder are 97.8%, 97.8% and 86.2% less that those for the smooth cylinder at Reynolds number of 1.0×10^{5}.

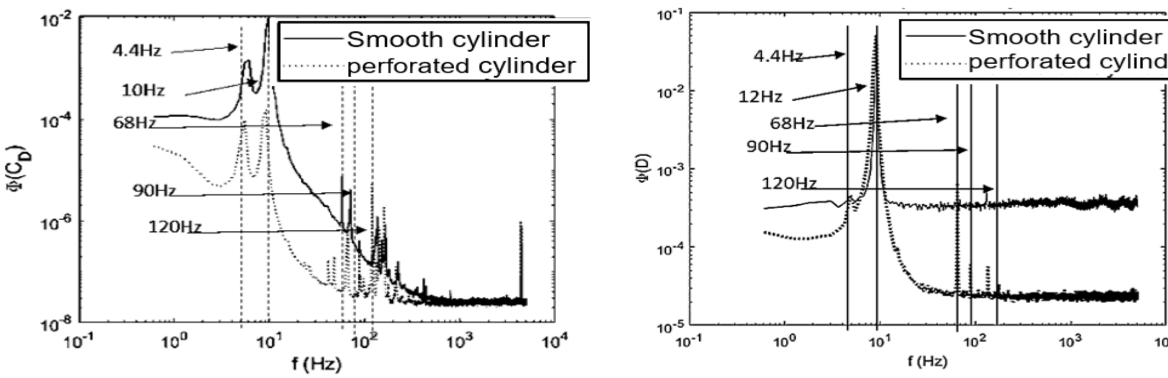

Figure 8 (Left) The PSD of Drag Coefficient of the unperforated and perforated cylinders at Reynolds number =1.0×10^{5}; and (Right) PSD of Drag of the unperforated and perforated cylinders acquired at U_∞ = 0.0 m/s (impact test).

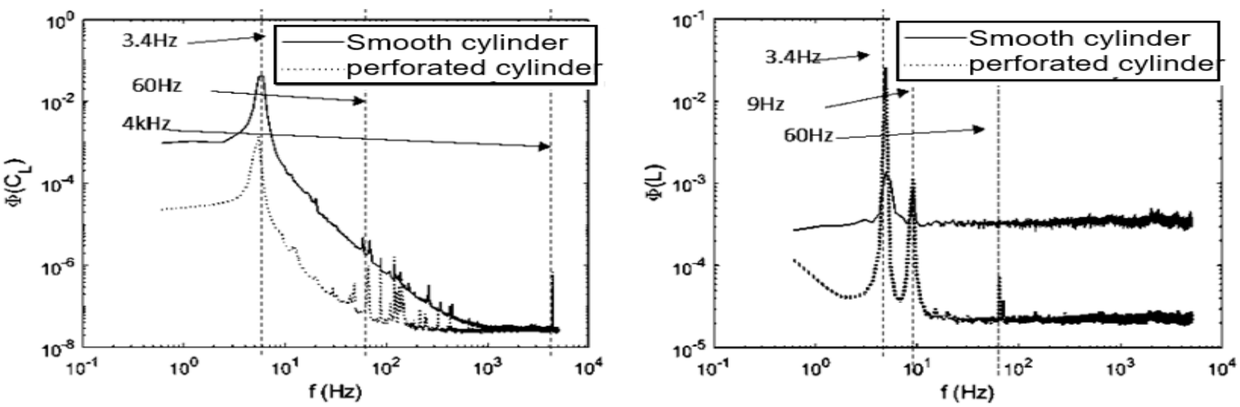

Figure 9 (Left) PSD of Lift Coefficient to Frequency of the unperforated and perforated cylinders for Reynolds number =1.0×10^{5}. (Right) PSD of Lift to Frequency of the unperforated and perforated cylinders at U_∞ = 0m/s (impact test)

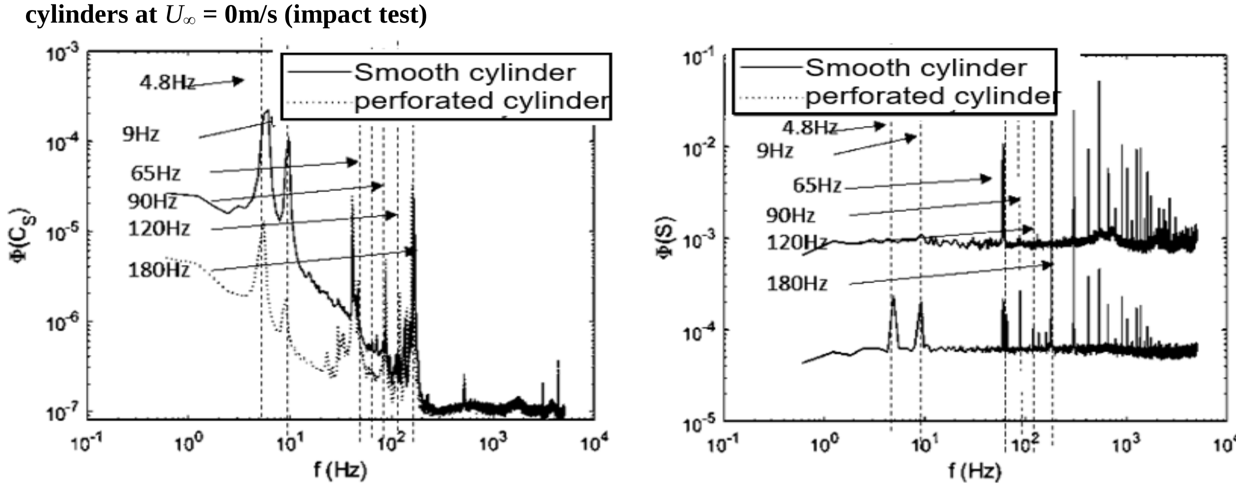

Figure 10 (Left) PSD of Side Force Coefficient to Frequency of the smooth and perforated cylinders for Reynolds number =1.0×10^{5}. (Right) PSD of Side Force to Frequency of the smooth and perforated cylinders at U_∞ = 0m/s (impact test)

B. Hot-wire wake survey results

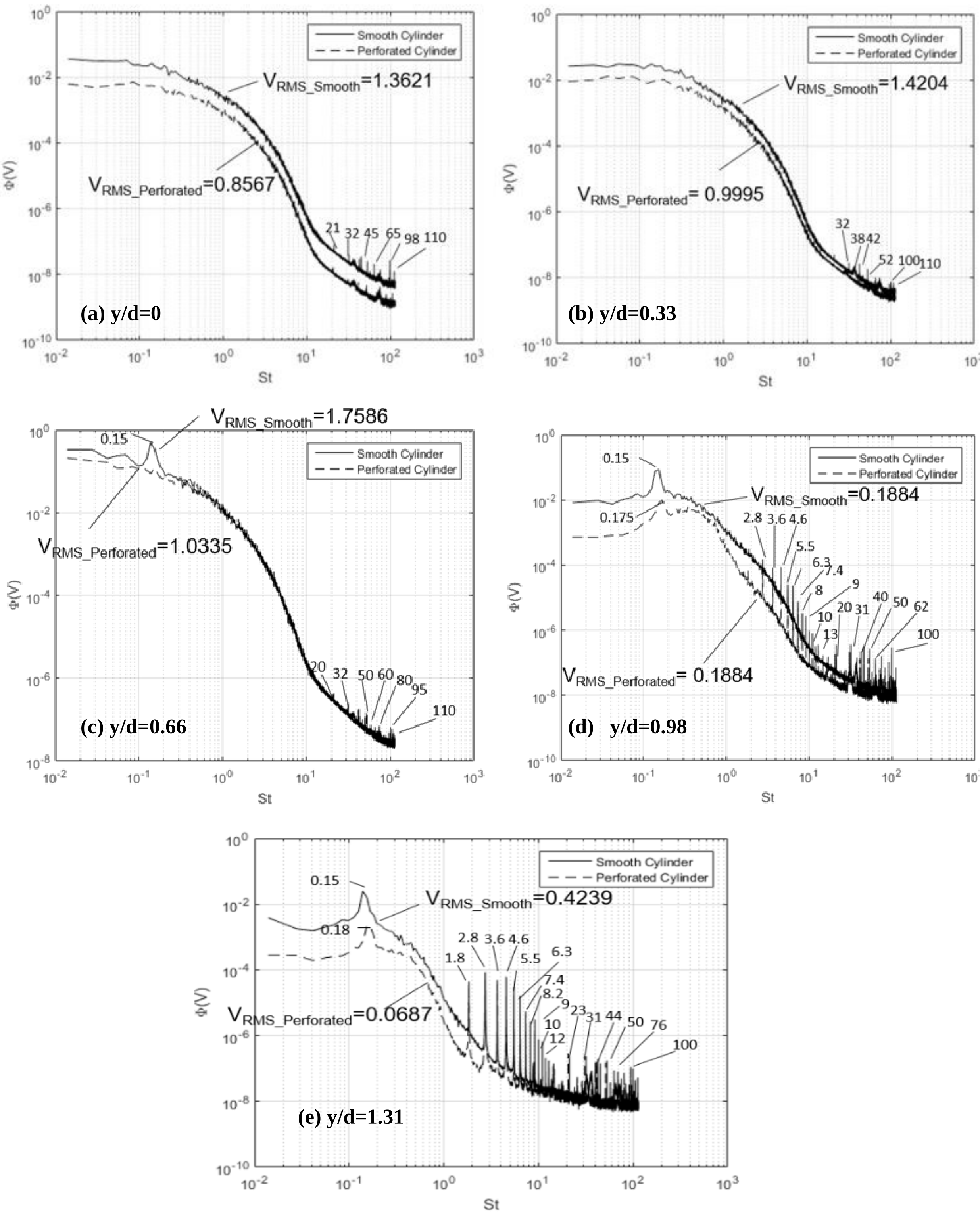

Figure 11 PSD of Velocity to Struohal number of the smooth and perforated cylinders at x/d=1.5. (a) y/d=0 (b) y/d=0.33 (c) y/d=0.66 (d) y/d=0.98 (e) y/d=1.31

Figure 11 shows the PSD of u-velocity versus Strouhal number based on the time series of the u-compoment velocity measured by using hot-wire anemometry at at x/d=1.5 in the cylinder wake. Figure 11(a) shows the result obtained at the center of the wake of the cylinder, thus the shedding frequency of $St = 0.20$ is not observed. As the traverse moves outward in the lateral direction of the wake, the peak freqency at $St = 0.20$ gradually shows up. The reduction in PSD for perforated cylinder at y/d=0, 0.33, 0.66, 0.98 and 1.31 are 37.11%, 29.63%, 41.23%, 88.23% and 83.79%, respectively comparing with the smooth cylinder. Clearly, the peak value of the spectrum plot occurring at $St = 0.20$ defines the shedding frequency of the cylinder at $Re = O(1.0\times10^5)$, which is in agreement with the classic data given in White[17] (2011). At x/d=1.5, the magnitude of the velocity spectrum of the perforated cylinder is always lower than the smooth cylinder. The high frequency oscillation in the spectrum plots can be seen in Figure 11 at y/d=0.98, and 1.31. This implies that asymmetric lee-wake vortex (Qui *et. al.*[19] , 2014) is formed in the separated shear layer.

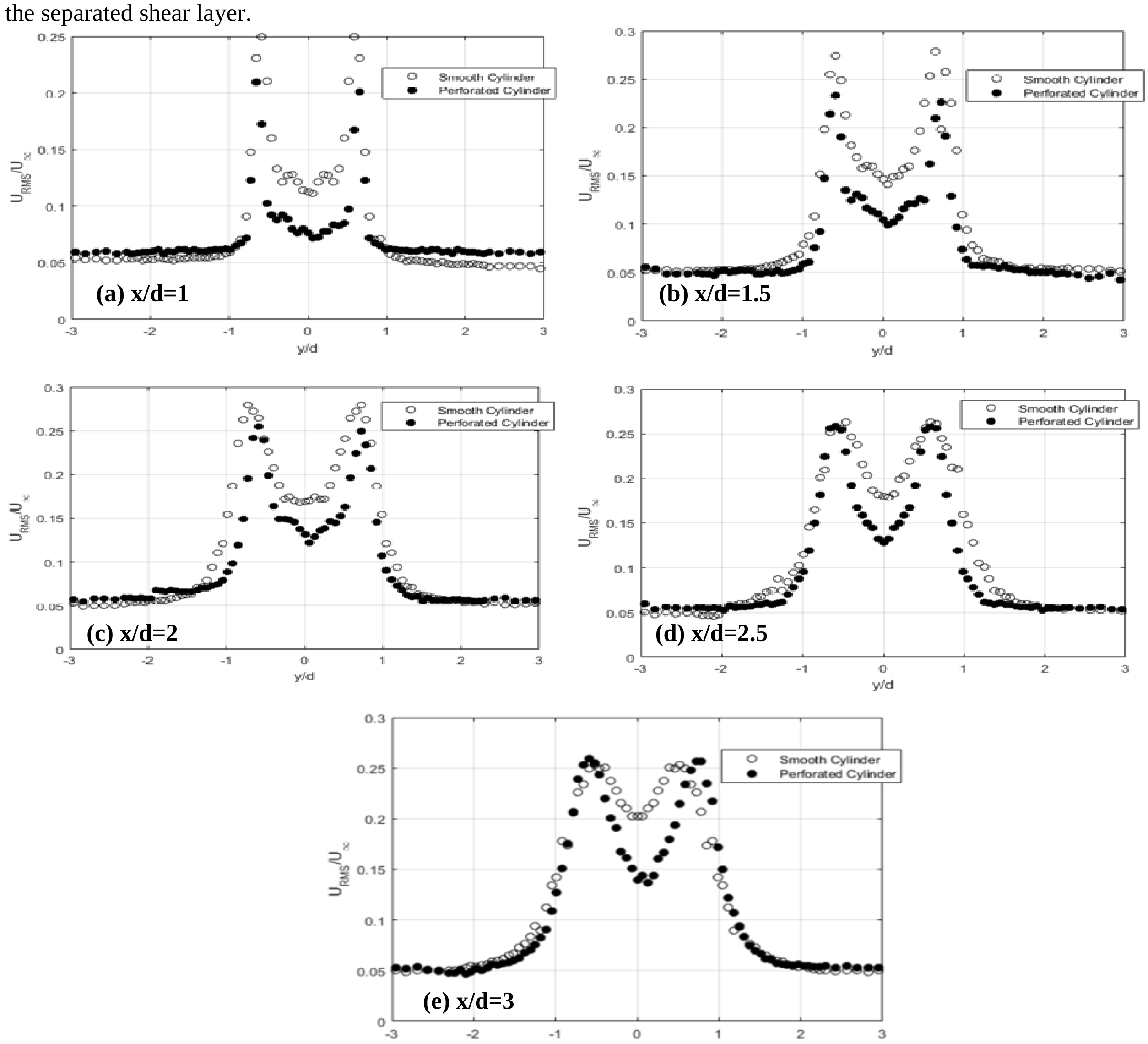

Figure 12 r.m.s. of Velocity to y/d from -3 to 3 of the smooth and perforated cylinders at (a) x/d=1 (b) x/d=1.5 (c) x/d=2 (d) x/d=2.5 (e) x/d=3

Figure 12 shows the comparisons of the r.m.s velocity profiles of the cylinder wake at different streamwise measurement stations. The r.m.s. velocity profile shows that the flow behind the cylinder is less turbulent for the perforated cylinder in comparison with the smooth cylinder. The perforated cylinder has a constantly lower r.m.s. velocity profile when compared with the smooth cylinder at all the x/d distances, as can be seen in Figure 12.

C. Uncertainty Analysis

To find the accuracy of the test results for the cylinder model, the uncertainty analysis has been conducted following the procedures implemented in Liu and Katz[20] (2018) based on Bendat and Piersol[21] (2012). This estimate will be used to find out the range in which the true mean value resides. As stated in Section II, for the range of Reynolds number 0.5×10^5 to 2×10^5, data has been analyzed from 10 statistically independent test sets for each Reynolds number. The ensemble mean of each data has been calculated using the equation below.

$$\bar{X} = \frac{1}{N}\sum_{k=1}^{N}\bar{X}_k \qquad (1)$$

where, $\bar{X}_k$ is the arbitrary dataset mean of the quantity X for a dataset k with k=1, 2, …, N, and N being the total number of data sets analyzed for the quantity X.

The standard deviation of an arbitrary dataset mean is calculated using the following relation.

$$S_{\bar{X}_k} = \sqrt{\frac{1}{N-1}\sum_{k=1}^{N}(\bar{X}_k - \bar{X})^2} \qquad (2)$$

Then, the standard deviation of the ensemble mean have $\bar{X}$ is calculated using following relation.

$$S_{\bar{X}} = \frac{1}{\sqrt{N}}S_{\bar{X}_k} = \sqrt{\frac{1}{N(N-1)}\sum_{k=1}^{N}(\bar{X}_k - \bar{X})^2} \qquad (3)$$

The probability level (a.k.a., confidence level) P% about the uncertainty range over which the ensemble mean value reside is given as

$$\bar{X} \pm t_{\nu,P}S_{\bar{X}} \qquad (P\%) \qquad (4)$$

where, $\nu = N - 1$ is the degree of freedom for standard deviation and t is the student's t variable. For the current experiment, with N=10, the corresponding "Student" *t* factor is $t_{9,95} = 2.262$ at 95% probability level. Then each of the ensemble mean value is normalized by the corresponding maximum absolute values of that quantity. Figure 13 compares the variation of the mean drag, lift and side force coefficients with Reynolds number, with error bars shown on the basis of the uncertainty analysis.

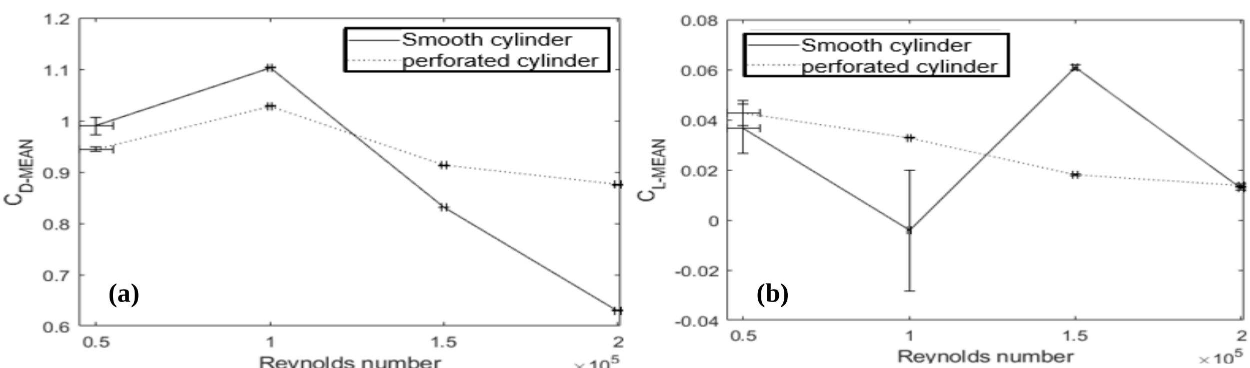

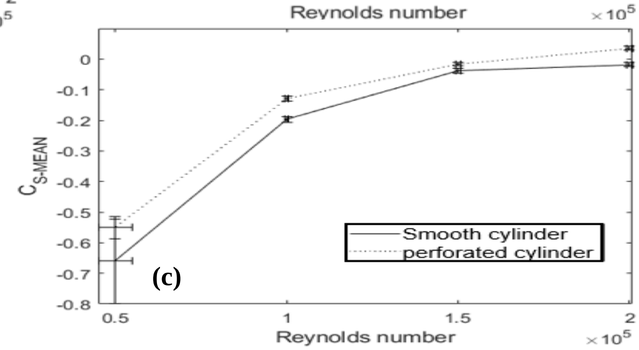

Figure 13 Comparison of C_{D_MEAN}, C_{L_MEAN} and C_{S_MEAN} versus Reynolds number between smooth and perforated cylinders with error bar as given in figures (a), (b), and (c) respectively.

The uncertainty analysis is conducted for the force measurement results at 95% probability level. As shown in Table 1 and Table 2, for mean and r.m.s. values of the drag, lift, and cylinder axial force (side force) coefficients, the peak relative uncertainty magnitude is less than 20%, except the high uncertainty level for mean lift coefficient for smooth cylinder due to unsteady oscillation at Reynolds number 1.0×10^5. The perforated cylinder does not oscillate at this Reynolds number, hence it has a lower uncertainty magnitude.

Figure 13 (a) & (c) shows that the error bars for C_{D_MEAN} and C_{S_MEAN} values at all Reynolds numbers tested are well within a very small relative uncertainty range, and the smooth and perforated cylinder results does not overlap on each other. As shown in Figure 13 (b) the large error bar of C_{L_MEAN} for the smooth cylinder at Re= 1.0×10^5 indicates the effect of resonance occurred at that Reynolds number.

Table 1. Uncertainty range ($\pm t_{9,95} S_{\bar{X}}$) of ensemble average values for the measured statistical quantities at 95% confidence level, normalized by the corresponding maximum absolute value for the smooth and the perforated cylinder.

Reynolds number	Statistical quantity of force coefficients $\bar{X}$	Smooth Cylinder	Perforated cylinder	$\lvert\bar{X}\rvert_{max}$ for smooth cylinder	$\lvert\bar{X}\rvert_{max}$ for perforated cylinder
Re=0.5×10^5	C_{Dmean}	±1.7%	±0.5%	1.01	0.95
	C_{Lmean}	±18.3%	±9.7%	0.054	0.051
	C_{Smean}	±16.6%	±6.0%	0.83	0.60
Re=1.0×10^5	C_{Dmean}	±0.1%	±0.1%	1.11	1.03
	C_{Lmean}	±34.1%	±1.5%	0.0047	0.0150
	C_{Smean}	±4.5%	±4.9%	0.21	0.14
Re=1.5×10^5	C_{Dmean}	±0.1%	±0.1%	0.47	0.52
	C_{Lmean}	±2.8%	±2.8%	0.037	0.0109
	C_{Smean}	±13.7%	±18.4%	0.058	0.0319
Re=2.0×10^5	C_{Dmean}	±0.2%	±0.1%	0.63	0.88
	C_{Lmean}	±3.3%	±4.1%	0.014	0.015
	C_{Smean}	±19.1%	±12.8%	0.037	0.045

Table 2. Uncertainty range ($\pm t_{9,95} S_{\bar{X}}$) of the r.m.s. values of the statistical quantities at 95% confidence level, normalized by the corresponding maximum absolute value for the smooth and the perforated cylinder.

Reynolds number	Statistical quantity of force coefficients $\bar{X}$	Smooth cylinder	Perforated cylinder	$\lvert\bar{X}\rvert_{max}$ for smooth cylinder	$\lvert\bar{X}\rvert_{max}$ for perforated cylinder
Re=0.5×10^5	C_{Drms}	±1.7%	±6.9%	0.32	0.072
	C_{Lrms}	±16.1%	±11.6%	0.32	0.091
	C_{Srms}	±1.0%	±0.7%	0.097	0.093
Re=1.0×10^5	C_{Drms}	±10.7%	±9.7%	0.17	0.028
	C_{Lrms}	±13.4%	±13.2%	0.14	0.026
	C_{Srms}	±4.2%	±1.4%	0.039	0.027
Re=1.5×10^5	C_{Drms}	±9.8%	±7.8%	0.061	0.011
	C_{Lrms}	±11.7%	±14.6%	0.14	0.023
	C_{Srms}	±4.5%	±3.6%	0.027	0.018
Re=2.0×10^5	C_{Drms}	±12.9%	±8.9%	0.048	0.016
	C_{Lrms}	±14.7%	±12.4%	0.104	0.033
	C_{Srms}	±4.2%	±7.1%	0.021	0.019

Conclusion

The unsteady aerodynamic loading on a smooth circular cylinder and a perforated circular cylinder with a hole diameter of 1.3% of the cylinder diameter and a porosity ratio of 8.25%, is investigated using load cells. The drag reduction effect of the surface performation method is further verified by a cylinder wake velocity profile survey by using hot-wire anemometry. For the Reynolds number range of 0.5×10^5 to 2.0×10^5 at an increment step of 0.5×10^5, the measurement results of the perforated cylinder were compared with those of the smooth cylinder. The r.m.s. values of C_D, C_L and C_S for the perforated cylinder are reduced by 81.78%, 84.54% and 26.18%, respectively in comparison with those of the smooth cylinder, indicating a corresponding beneficial reduction in flow-induced vibration, which is confirmed from the visual inspection. The peak of the power spectrum of C_D for the perforated cylinder is reduced by almost 2 octaves in comparison with the smooth cylinder on load cell measurement.

Hot wire measurement results show that, significant reductions for velocity r.m.s. fluctuations were achieved for the perforated cylinder in comparison with the smooth one, with 9% reduction at the edge of the wake and 32% reduction at the center of the wake. Spectral analysis at various locations across the cylinder wake also indicates an overall reduction in fluctuation amplitude across the spectrum for the perforated cylinder when compared with the smooth cylinder. Also, comparison of the hotwire velocity measurement results indicates a 12% to 76% reduction in the u-component normal stress, confirming the reduction in unsteady aerodynamic loading.

Except the high uncertainty level (±34.1%) due to high level unsteadiness for the mean C_L of the smooth cylinder at Re=1.0×10^5, the uncertainty levels for the mean and r.m.s aerodynamic force components are negligible.

References

[1]Price, P., “Suppression of the Fluid-Induced Vibration of Circular Cylinder,” *Journal of Engineering Mechanics Division, American Society of Civil Engineers*, Vol. 82, No. 1030, 1956, pp. 1-22.

[2]Pinar, E., Ozkan, G. M., Durhasan, T., Aksoy, M. M., Akilli, H., and Sahin, B., “Flow Structure Around Perforated Cylinders in Shallow Water,” *Journal of Fluids, and Structures*, Vol. 55, 2015, pp. 52-63.

[3]Homann, F., “The Influence of High Viscosity on the Flow Around the Cylinder and Around the Ball,” *Journal of Applied Mathematics and Mechanics*, Vol. 16, No. 3, 1936, pp. 153-164.

[4]Zdravkovich, M. M., “Conceptual Overview of Laminar and Turbulent Flows Past Smooth and Rough Circular Cylinders,” *Journal of Wind Engineering and Industrial Aerodynamics*, Vol. 33, No. 1-2, 1990, pp. 53-62.

[5]Lin, J. C., Towfighi, J., and Rockwell, D., 1995, "Instantaneous Structure of the Near-Wake of a Circular Cylinder: On the Effect of Reynolds Number," *Journal of Fluids and Structures*, Vol. 9, No. 4, 1995, pp. 409-418.

[6]Norberg, C., "LDV-Measurements in the Near Wake of a Circular Cylinder," *Summer Conference Proceeding of Fluids Engineering Division*, ASME, Washington, DC, 1998, pp. 1-12.

[7]Rajagopalan, S., and Antonia, R., "Flow Around a Circular Cylinder—Structure of the Near Wake Shear Layer," *Experiments in Fluids*, Vol. 38, No. 4, 2005, pp. 393-402.

[8]Dong, S., Karniadakis, G., Ekmekci, A., and Rockwell, D., "A Combined Direct Numerical Simulation–Particle Image Velocimetry Study of the Turbulent Near Wake," *Journal of Fluid Mechanics*, Vol. 569, 2006, pp. 185-207.

[9]Prasad, A., and Williamson, C. H. K., “The Instability of the Shear Layer Separating from a Bluff Body,” *Journal Fluid Mechanics*, Vol. 333, 1997, pp. 375-402

[10]Ozgoren, M., Pinar, E., Sahin, B., and Akilli, H., 2011, "Comparison of Flow Structures in the Downstream Region of a Cylinder and Sphere," *International Journal of Heat and Fluid Flow*, 32:6, 2011, pp. 1138-1146.

[11]Ozkan, G. M., Firat, E., and Akilli, H., 2017, "Control of Vortex Shedding Using a Screen Attached on the Separation Point of a Circular Cylinder and Its Effect on Drag," *Journal of Fluids Engineering*, ASME, Vol. 139, No. 7, 2017, pp. 1-11.

[12]Ozkan, G. M., Oruc, V., Akilli, H., and Sahin, B., “Flow Around a Cylinder Surrounded by a Permeable Cylinder in Shallow Water,” *Experimental Fluids*, Vol. 53, No. 6, 2012, pp. 1751-1763.

[13]Gozmen, B., Akilli, H., and Sahin, B., “Vortex Control of Circular Wake by Permeable Cylinder,” *Cukurova University Journal of the Faculty of Engineering and Architecture*, Vol. 28, No. 2, Dec. 2013, pp. 77-85.

[14]Pinar, E., Durhasan, T., Ozkan, G. M., Aksoy, M. M., Akilli, H., and Sahin, B., “The Effect of Perforated Cylinders on the Vortex Shedding on the Suppression of a Circular Cylinder,” *EPJ Web of Conference*, Vol. 143, 2017, pp. 02094-02101.

[15]Durhasan, T., Aksoy, M. M., Pinar, E., Ozkan, G. M., Akilli, H., and Sahin, B., “Vortex Street Suppression of a Circular Cylinder using Perforated Semi-Circular Fairing in Shallow Water,” *Experimental Thermal and Fluid Science*, Vol. 79, 2016, pp. 101-110.

[16]Chen, W. L., Xin, D. B., Xu, F., Li, H., Ou, J. P., and Hu, H., “Suppression of Vortex-Induced Vibration of a Circular Cylinder Using Suction-Based Flow Control,” *Journal of Fluids and Structures*, Vol. 42, 2013, pp. 25–39.

[17]White, F. M., “Viscous Fluid Flows,” 3rd ed., McGraw-Hill, New York, 2011, pp. 10-15.

[18]Wieselsberger, C., “New Data on the Laws of Fluid Resistance,” NACA TN - 84, Vol. 22, March 1922, pp. 321-328.

[19]Qiu, Y., Sun, Y., Wu, Y., and Tamura, Y., “Effects of Splitter Plates and Reynolds Number on the Aerodynamic Loads Acting on a Circular Cylinder,” *Journal of Wind Engineering & Industrial Aerodynamics*, Vol. 127, 2014, pp. 40-50.

[20]Liu, X., and Katz, J., “Pressure–Rate-of-Strain, Pressure Diffusion and Velocity– Pressure-Gradient Tensor Measurements in a Cavity Flow,” *AIAA Journal*, 56, no. 10 (2018): 3897-3914.

[21]Bendat, J. S., and Piersol, A. G., “Random Data: Analysis and Measurement Procedures,” 4th ed., Wiley, New York, 2012, pp. 249-287.